Autism Spectrum Disorder characterization in children by capturing local-regional brain changes in MRI

Charlems Alvarez-Jimenez[1,2], Nicolás Múnera-Garzón[1,2],
Maria A. Zuluaga[4,1], Nelson F. Velasco[1,2,3], Eduardo Romero[1,a)]

[1] Computer Imaging and Medical Application Laboratory - CIM@LAB, Universidad Nacional de Colombia, Bogotá, 111321, Colombia.
[2] ACCEDER Group, Universidad Militar Nueva Granada, Bogotá, 110111, Colombia.
[3] GIDAM Group, Universidad Militar Nueva Granada, Bogotá, 110111, Colombia.
[4] Data Science Department, EURECOM, Biot, 06410, France.

Version typeset October 30, 2019

[a)] Author to whom correspondence should be addressed. Electronic mail: edromero@unal.edu.co

Purpose: To design a multiscale descriptor capable of capturing complex local-regional unfolding patterns to support quantification and diagnosis of Autism Spectrum Disorders (ASD) using T1-weighted structural magnetic resonance images (MRI) with voxel size of $1 \times 1 \times 1$ mm.

Methods: The proposed image descriptor uses an adapted multiscale representation, the Curvelet transform, interpretable in terms of texture (local) and shape (regional) to characterize brain regions, and a Generalized Gaussian Distribution (GGD) to reduce feature dimensionality. In this approach, each MRI is first parcelled into 3D anatomical regions. Each resultant region is represented by a single 2D image where slices are placed next to each other. Each 2D image is characterized by mapping it to the Curvelet space and each of the different Curvelet sub-bands is described by the set of GGD parameters. To assess the discriminant power of the proposed descriptor, a classification model per brain region was built to differentiate ASD patients from control subjects. Models were constructed with support vector machines and evaluated using two samples from heterogeneous databases, namely *Autism Brain Imaging Data Exchange* - ABIDE I (34 ASD and 34 controls, mean age 11.46 ± 2.03 and 11.53 ± 1.79 years respectively, male population) and ABIDE II (42 ASD and 41 controls, mean age 10.09 ± 1.37 and 10.52 ± 1.27 years respectively, male population), for a total of 151 individuals.

Results: When the model was trained with ABIDE II sample and tested with ABIDE I on a hold-out validation, an area under receiver operator curve (AUC) of 0.69 was computed. When each sample was independently used under a cross-validation scheme, the estimated AUC was 0.75 ± 0.02 for ABIDE I and 0.77 ± 0.01 for ABIDE II. This analysis determined a set of discriminant regions widely reported in the literature as characteristic of ASD.

Conclusions: The presented image descriptor demonstrated differences at local and regional level when high differences were observed in the Curvelet sub-bands. The method is simple in conceptual terms, robust to several sources of noise and has a very low computa-

i

tional cost.

Keywords: MR Quantitative imaging, Texture analysis, Computer-aided decision support systems

I.   Introduction

Autism Spectrum Disorders (ASD) are complex neuro-developmental conditions that manifest during the first three years of life[1]. Commonly, affected children exhibit repetitive patterns, limitations in social interaction and communication skills[2,3]. In 2014, an average of 1 out of 59 children in the United States was identified as having this disorder (only at age eight)[4].

Post-mortem brain studies have shed some light on the physiopathology of this disorder. Histochemical, autoradiographic and biochemical tests have established differences between ASD patients and control individuals[5]. These tests demonstrate pathological differences at local (cellular) and global (region or whole brain) levels, i.e., reduced neuronal size and cell density loss in some brain regions like hippocampus[6], cerebellum[7], amygdala[8], as well as age related changes that produce increased gray/white matter and increased cortical thickness as a result of dysregulated pruning[9], or atypical sulcal anatomy in young children with ASD[10]. In addition, other studies have described morphometric cortical abnormalities in people with autism, specifically shape changes at the level of the corpus callosum, the central, intraparietal and frontal medial sulci[10,11]. Unfortunately, these findings have no relevance in clinical practice and are completely ignored in radiological examinations, even though Magnetic Resonance Imaging (MRI) has been reported as the most used technique to understand ASD[1]. The main bottleneck consists in the lack of quantitative features that can provide evidence of the state of the disease.

Different studies have attempted to determine brain changes mainly using morphometry[12,13,14,15] and texture feature analysis[16,17]. Morphometry is applied under the hypothesis that there exists a significant variation in terms of shape, contour and volume of certain brain regions[12,14,15]. For instance, Sato *et al.*[15] proposed a voxel-based morphometry strategy that revealed reduced gray matter volume in a particular set of regions in adults with ASD, most of these regions constituting the social brain network. Interestingly, classification

performance was better when using this set of regions. Similarly, Retico *et al.*[14] computed morphometric features such as volume, curvature, regional width and depth to perform a classification task for differentiating between ASD and control subjects using Support Vector Machines (SVM), while Giulianoa *et al.*[12] used five surface-based features to morphologically describe brain regions. Likewise, texture features have been commonly used to describe brain regions by considering the variability of gray and white matter between ASD and control individuals[16,17]. As an example, Chaddad *et al.*[16] described brain regions by extracting multiscale texture features (entropy, mean and standard deviation) using Laplacian of Gaussian (LoG) filters, and performed a statistical analysis to identify the regions that show higher differences between ASD patients and control subjects.

The main contributions of this work are:

- Use of Curvelet transform to characterize regions with Generalized Gaussian Distribution to reduce feature dimensionality.

- Quantification of local-regional changes in anatomic brain regions by a *2D multislice image*, aiming to capture relationships of a region in the Curvelet space that describe atypical brain folding.

- Evaluation in heterogeneous datasets which proves the method can be generalized.

Recent evidence has demonstrated ASD patients may exhibit atypical brain folding patterns as an early manifestation of the altered neurodevelopmental process[10]. This resultant cortex wrapping should be thought of as not only a change of the volumetric shape but rather as an alteration of the topological regional relationships. Highlighting such patterns is not an evident task since differences need not necessarily be determined at the level of first-order relationships (typical 3D analysis). The approach herein proposed is basically a 2D analysis by mapping the set of 2D slices of a 3D region to the same plane (a 2D multislice image) and capturing their different relationships by a general transformation. Therefore, this investigation introduces a multiscale descriptor that characterizes 3D brain regions and highlights those ones with differences between ASD patients and control subjects in MRI studies. Characterization of a brain region is performed by applying the Curvelet transform to the 2D multislice image, the base of the multiscale analysis, where information is frequency-decomposed into a set of sub-bands along different scales and orientations. The

Last edited $Date$: October 30, 2019

coefficient distribution of each Curvelet sub-band is approximated by a parametric function, characterizing any sub-band with only three parameters, an important dimensionality reduction. The proposed approach was validated by automatically classifying ASD and control children populations belonging to heterogeneous datasets from the *Autism Brain Imaging Data Exchange* (ABIDE)[18,19], which could help towards generalization.

II.   Materials and Methods

The main goal of this work was to devise an image descriptor that captures local and regional brain changes, aiming thereby to estimate both regional shape alterations and possible cellularity losses[7,8,20,21]. The resultant descriptor was validated by a conventional classification task, which tests the representation aptness to discriminate between control and ASD cases.

II.A.   Data

Data for this investigation are part of the *Autism Brain Imaging Data Exchange* (ABIDE)[18], an open project including cases collected from 17 institutions, with patients aged between 5 and 64 years: a total of 1112 cases from ABIDE I[18] and 1114 cases from ABIDE II[19]. This study only considered cases corresponding to children between 6 and 13 years, and the purpose of this partition is to analyze and identify pathologic patterns (from ASD children population) that differ from the normal brain growth (represented by control population), and therefore allows early diagnosis. This study includes cases with structural T1-MRI scans with a voxel size of $1 \times 1 \times 1$ mm.

The ABIDE I sample consists of 34 ASD patients and 34 control subjects between 5 and 13 years (mean age 11.46 ± 2.03 and 11.53 ± 1.79 years respectively). In addition, all the children in this sample correspond to male individuals. These cases were collected from six different centers (see Table 1). The use of data from multiple centers implies that the available set of images is different in terms of number of slices per volume, inter-slice distance, image resolution and scanner protocol. The ABIDE II sample is composed of 42 ASD patients and 41 control subjects with ages between 7 and 12 years (mean age 10.09 ± 1.37 and 10.52 ± 1.27 years respectively). In addition, all children in this sample also correspond to male individuals collected from four different centers (see Table 1). Note two of the

---

Last edited $Date$: October 30, 2019

four centers for the ABIDE II sample are different from the ones in the ABIDE I sample. In addition, the population distribution is quite different. Finally, Table 1 also shows the scanner model used in each of the centers where the structural magnetic resonance images were acquired, demonstrating data heterogeneity.

II.B. Methods

The pipeline of the proposed strategy is shown in Figure 1. The principle behind this characterization strategy is that differences between local brain patterns should be observable among different scales. Overall, pre-processing aims to normalize image intensities, remove the skull and segment each case into a set of brain regions. In a second phase, each segmented region (a volume) is mapped to a 2D image by orderly placing upon it each of the volume slices. This 2D image with the collection of slices is analyzed using the Curvelet transform, and the coefficient distribution per Curvelet sub-band is approximated by a Generalized Gaussian Distribution. Therefore, each sub-band ends up by being represented by three parameters. Finally, to evaluate the ability of the constructed multiscale descriptor to differentiate the two classes, a conventional SVM performs a binary classification per region and those regions related with ASD are identified.

II.B.1. Preprocessing

The preprocessing phase is carried out per brain magnetic resonance imaging using *FSL* software and involves the following steps: a) intensity normalisation (FSLMATHS tool[22]), b) skull removal (Brain Extraction Tool (BET)[23]), c) rigid-elastic registration from the MNI152 template to each brain in the dataset (FLIRT-FNIRT tools[24,25]), and d) the Harvard Oxford atlas[26] is registered to each brain using the previously computed elastic transformation matrix, and thereby providing a segmentation mask with 117 regions (96 cortical and 21 sub-cortical).

II.B.2. Multiscale descriptor

The construction of the multiscale descriptor per region is illustrated in Figure 1.B and herein explained.

Last edited $Date$: October 30, 2019 II.B. Methods

Volume representation: For each segmented brain region, the 3D image is mapped to a 2D mosaic, called the *2D multislice image*. This new image corresponds to the 3D region mapped to a 2D plane, as illustrated in Figure 1.B.1, independently of the number of slices or the size of the region. The obtained mosaic is then zero-padded to fit a squared shape, necessary for the Curvelet characterization. This representation captures main topological relationships of a region in the Curvelet space and can describe structural changes like atypical brain folding without losing of the relevant 3D information. From this point of view, features in this space are not necessarily correlated with measures like surface area, thickness or folding[27,28], since the object basic relationships in the Curvelet space do not have the usual Euclidean geometric meaning. Several studies have reported differences with these measures, but the approach herein presented rather attempts to capture subtle anatomic changes manifested by loss of the global shape which are hardly detected as size or volume alterations. Note each 2D multislice image size is variable to conserve original information and depends on: i) the particular brain region of analysis, ii) the number of slices such region contains, and iii) the image resolution provided by the scanner.

Multiscale Analysis: The multiscale analysis is performed by transforming the 2D multislice image to the Curvelet space (as shown in Figure 1.B.2), a transformation introduced by its well demonstrated aptness to approximate textures and complex geometrical structures[29]. The Curvelet transformation is a multiscale geometric mapping that preserves the same good decomposition advantages reported with the Wavelet transform[30], but introducing a compact representation of curved geometric structures. In fact, Curvelet functions are known for giving sparse representations of smooth objects with discontinuities along curves[29]. In this work, the Curvelet representation allows to describe brain regions in terms of their local/regional differences between ASD patients and control subjects.

A Curvelet frequency space is defined by the convolution between radial $R(\omega)$ and angular $\Phi(\omega)$ windows, being $R(\omega)$ the scale and $\Phi(\omega)$ the phase along the radial direction[31]. The object proportion between different scales is ensured by the special scaling law $width \approx length^2$, i.e., anisotropy increases as long as scales decrease. In terms of a dyadic spatial decomposition, a Curvelet is characterized by two levels of location: a coarse location in the usual dyadic spatial square and a finer one which anisotropically places the Curvelet within such coarse dyadic square. The term micro-location refers to this finer placement.

II.B.   Methods

In addition, the anisotropy property rises two relations, the number of directions and the number of micro-locations are both proportional to the inverse of the scale. This anisotropic characterization of curves was the main motivation to select this representation since we seek to capture distortions of the regional and local shapes. In addition, the proportionality of number of micro-locations with respect to the scale, results crucial to characterize particular texture patterns which are herein supposed to describe tissular arrangements that correlate with the neuropathology. In the Curvelet frequency representation, the scaling law amounts to refine directions every two scales, and the wedge (sub-band) coefficients represent the parabolic relationship for a given scale

This work characterizes brain regions by using the Fast Discrete Curvelet Transform (FDCT), configured by defining the optimal number of scales and angles to perform the experiments. Since the scale is a resolution-dependent parameter and the smallest resolution of the 2D mustislice images in the dataset is 96×96 pixels, the maximum number of scales to be used is 4. Regarding the number of angles, 16 has been reported to achieve the best results for this particular representation[32]. Therefore, the FDCT representation is split along 4 scales in 16 different angles, i.e., due to the dyadic decomposition a set of 81 Curvelet sub-bands are provided.

Dimensionality Reduction: Each sub-band (wedge) contains a set of coefficients that describes a specific range of frequencies at a particular scale and a determined orientation. Note that the number of coefficients per sub-band varies according to: i) size of the 2D multi-slice image and ii) the particular scale and orientation of analysis. Therefore, the Generalized Gaussian Distribution (GGD) is used in this investigation to approximate each coefficient distribution with three parameters, achieving an important dimensionality reduction as well as unifying the size of the feature vector that describes each brain region. This parametric approximation meets each set of coefficients as either a Laplacian, normal or flat distributions (see Figure 2). This distribution has demonstrated to give accurate descriptions of the Wavelet or Curvelet coefficients for a given sub-band[30,33]. In a GGD, μ stands for the mean of the distribution, β models the decay rate from the peak, ρ models the peak width (like the standard deviation σ in a Gaussian distribution) and Γ corresponds to the gamma function[34]. Therefore, the GGD is used in this work to approximate the set of coefficients per Curvelet sub-band by 3 parameters (as shown in Figure 1.B.3). Since 81 sub-bands are

computed, a feature vector of 243 components characterizes each brain region.

II.B.3. Classification

Support Vector Machines (SVM), a discriminant binary classifier[35], is used to build a model for each brain region. SVM provides a mapping of each element onto a space, which may establish a linear or non-linear boundary between two classes, as wide as possible. The underlying strategy, the kernel trick, consists in mapping data by a kernel function. A kernel is a function $k : X \times X \to R$ associated to a mapping $1, \ldots, \phi : X \to F$ such that $\forall\, x, y \in X, k(x, y) = \langle \psi_1(x), \psi_1(y) \rangle_F$, i.e., k calculates the dot product in F. Intuitively, a kernel may be thought of as a function that measures similarity between two objects of the input space. In this work, a binary SVM model per region is trained using the a matrix of $f \times n$ size, where f corresponds to 243 features computed in the previous phase (the proposed multiscale descriptor) and n stands for the total of cases (ASD patients and control subjects). Each region is independently analyzed to quantify how discriminative is to separate the two classes based on the proposed multiscale representation. The SVM is configured using two parameters, box-constraint and sigma. The box-constraint controls the penalty imposed to observations with large residuals while the sigma parameter defines how linear is the SVM decision boundary. For setting SVM parameters, a Bayesian optimization[36] is run over to find the best possible values for sigma and box-constraint. In addition, SVM models are tested with two different kernels, specifically a linear function and a radial basis function (RBF).

II.C. Evaluation

The set of experiments are hereafter described. The aim of these experiments is not to provide a final classification per subject but rather to find out a set of anatomical brain regions with pathological patterns, in terms of texture features, that describe and quantify this disorder.

Experiment 1: The aim of this experiment is to evaluate the ability of the proposed multiscale descriptor to differentiate ASD patients from control subjects with a data set never seen by the trained model. For so doing, ABIDE II sample (83 cases) is used for training

---

the classification model which is then tested with the sample of ABIDE I (68 cases) under a hold-one-out validation scheme (cases are individually tested). Classification performance is assessed by computing the area under the receiver operating characteristic curve (AUC), since most of state-of-the-art methods report such metric.

Experiment 2: The aim of this experiment is to identify the most discriminant regions in the classification task (ASD patients vs. control subjects), defined as the ability of a region to separate both classes. For each of the 117 regions, 10 iterations of 10-fold (one fold is held-out for testing) cross validation are carried out. Then, for each of the ten iterations, the 117 regions are sorted out by their AUCs, following a descendent order. The first ten regions are chosen for the 10 iterations: a region is then discriminant if this is present at least in 7 out of the 10 iterations. Test 2.a is performed for identifying discriminant regions using ABIDE I sample, while Test 2.b does the same using ABIDE II sample.

Experiment 3: The aim of this experiment is to illustrate the ability of the proposed representation to highlight differences between ASD patients and control subjects under certain conditions. Test 3.a seeks to visualize global shape differences or local textural patterns by using information from one sub-band (Curvelet coefficients), and Test 3.b seeks illustrates how the Curvelet sub-band distribution is independent of the particular age or scanner. For this evaluation, the highest scoring regions from Experiment 2 are selected as well as the associated Curvelet sub-bands showing significant differences between the two groups.

Experiment 4: The aim of this experiment is to compare the proposed representation with three classic measures (normalized volume, thickness and curvature), which have been broadly used for identifying brain regions that exhibit differences between ASD and control individuals[27,28]. Test 4.a presents classification performance using separately four descriptors (the proposed one and each classic measure), and Test 4.b computes and illustrates the correlation between the Curvelet descriptor and the three classic measures.

III. Results

III.A. Experiment 1

Figure 3 shows the classification results when the model is trained with the ABIDE II sample and tested with the ABIDE I under a hold-one-out validation scheme (cases individually tested), obtaining AUC scores of 0.69 (right parahippocampal gyrus) and 0.65 (left inferior frontal gyrus) with an RBF and a linear kernel, respectively. In addition, sensitivity of 0.77 and specificity of 0.59 were obtained when using an RBF kernel. The RBF kernel model outperformed the linear one. In addition, regions with the highest AUC scores are illustrated within each brain. Interestingly, an AUC score of 0.69 demonstrates this model is quite robust to different sources of variability since ABIDE is a non-homogeneous data set, i.e., this is multicentric data collection.

III.B. Experiment 2

Test 2.a: Figure 4 illustrates the resultant discriminant brain regions when using the ABIDE I sample: the upper two brains illustrate regions obtained with an RBF kernel, while the bottom ones show regions obtained with a linear kernel. This test provided regions widely reported as related with ASD, like caudate, inferior frontal gyrus, temporal occipital fusiform cortex and angular gyrus[37,38,39], the three latter regions also showed up in Experiment 1. Interestingly, the set of discriminant regions and estimated AUC scores are quite similar independently of the particular used kernel, i.e., the proposed descriptor yields an average AUC of 0.75 ± 0.03 (95% confidence interval: $0.74 - 0.78$) for the right supramarginal gyrus (anterior division) with an RBF kernel, and an average AUC of 0.75 ± 0.02 (95% confidence interval: $0.74 - 0.77$) with a linear kernel for the same region, as shown in Figure 4. In addition, sensitivity/specificity scores of $0.68/0.71$ and $0.76/0.82$ were obtained for this top region when using an RBF and a linear kernel, respectively.

Test 2.b: Similarly, Figure 5 shows the resultant discriminant regions when using the ABIDE II sample. The brains represent results obtained when the SVM model is trained with an RBF or a linear kernel. Some of the resultant regions have been reported as being related to ASD, such as superior temporal gyrus and temporal fusiform cortex[40,41], the latter also

showed up in Experiment 1. AUC scores and the associated standard deviations are shown at the bottom of the figure. Note the proposed multiscale descriptor provided an average AUC of 0.77 ± 0.04 (95% confidence interval: $0.75 - 0.80$) for the left superior temporal gyrus (anterior division) when using an RBF kernel, and 0.77 ± 0.04 (95% confidence interval: $0.74 - 0.80$) for the same region with a linear kernel, as shown in Figure 5. In addition, sensitivity/specificity scores of 0.73/0.80 and 0.74/0.71 were obtained for this top region when using an RBF and a linear kernel, respectively.

III.C. Experiment 3

Test 3.a: Figure 6 shows the visual differences when using two brain regions, the right supramarginal gyrus (A) and the left superior temporal gyrus (B), specifically using a sub-band located at the $4th$ scale and $\frac{9\pi}{8}$ of orientation. For each block, the first row corresponds to ASD patients while the second one stands for control subjects. The first two columns illustrate the selected region and the third column shows the reconstructed region volume after using only the relevant Curvelet sub-band. The Curvelet is by nature a multiscale representation, and therefore it naturally separates spatial information at different levels of resolution or scales. The aim of this analysis is then to highlight differences at several scale levels and characterize this disorder in terms of global shape differences or local textural patterns. The purpose of this figure is not an interpretation of the differences, but rather an illustration of the larger visual differences between the two reconstructed versions of analysis in the third column than between the two figures in the second column.

Test 3.b: Figure 7 illustrates the spread parameter for 3 Curvelet sub-bands (the ones with $p-value < 0.01$) from the left superior temporal gyrus. In this figure, each column represents one of the three sub-bands (the standard deviation of the GGD) as follows: first row displays the two groups, ASD (green) and control (orange) subjects, while second and third rows represents the same groups (same color convention) but distributed by age and scanner (center), respectively. This test demonstrates the same curved characteristic is shifted for the two groups, in this case subtle shape differences. Specifically, first and second rows demonstrate separability between ASD and control individuals independently of their age following a particular trend, i.e., ASD overall show lower values w.r.t. controls. Regarding

scanner, similar values are observed between the group of controls, yet the third and fourth centers report only two and one individuals, respectively. This analysis was extended by performing an ANOVA test, restricted by the differences in the number of subjects among centers, i.e., three rounds of ANOVA evaluations were performed between the two centers with at least ten individuals as follows: 11 cases from GU vs three random sets of 11 cases from KKI. All computed p-values demonstrate there are no significant differences between scanners: p-values were higher than 0.05 (0.98, 0.49 and 0.99).

III.D.   Experiment 4

Test 4.a: Normalized volume was computed with the same parcellation used in the proposed approach, the Harvard-Oxford atlas (HO)[26], while thickness and curvature were computed with a different parcellation, the Desikan Killiany atlas (DKT)[42] since FreeSurfer[43], a widely used software, has already implemented a standard pipeline for computing these measures. Because of the use of two atlas, an approximated relation between them was established. A SVM model was separately trained per descriptor. Table 2 shows the comparison between the proposed Curvelet approach and each computed measure. In this table, first column stands for the relevant regions with HO atlas (obtained in Test 2.b) while the fourth one stands for the approximated regions in the DKT atlas. The remaining columns presents AUC scores when using: Curvelet approach (second), normalized volume (third), thickness (fifth), and curvature (sixth). As expected, the classification performance between the Curvelet approach and each classic measure was quite different, suggesting the proposed representation captures different brain features and patterns, probably local-global discontinuities of the curves outlining the region, not only geometric global estimations like the curvature or the thickness.

Test 4.b: All the Curvelet sub-bands from the left superior temporal gyrus were analyzed by computing the *Pearson correlation coefficient* between each sub-band and each classic measure. Figure 8 illustrates these results for 3 Curvelet sub-bands ($p < 0.01$, *t-test*), evidencing nonlinear correlation between the Curvelet representation and each of the traditional measures. This analysis confirmed the Curvelet approach and the computed measures are describing brain regions in different ways, i.e., while the normalized volume is capturing

differences in terms of the region size without any information about shape or the curvature characterizes a region by approximating a global folding of the surface, the Curvelet approach instead is describing local and regional curves and their edges and discontinuities at different neighboring levels.

III.E.   Computational performance

All the experiments were implemented in MATLAB R18a (Mathworks Inc.), running on a Centos Server with 2 Intel Xeon CPU at 2.2 GHz and 256 GB of RAM. Computational performance was separately assessed by the two processes required to compute the proposed descriptor, namely the multiscale analysis and the dimensionality reduction. Brain regions were described using the 2D Fast Discrete Curvelet Transform (FDCT) implementation (approximately $195.7\,ms$ per case) while the dimensionality reduction was performed using the Generalized Gaussian Distribution (about $52\,ms$ per case). Therefore, computational time for running the proposed descriptor per case is approximately $0,25\,s$, a quite low computational cost.

IV.   Discussion

This work introduces a multiscale descriptor that characterizes anatomical brain regions in terms of their very basic geometric properties and highlights those ones with differences between ASD and control subjects. This descriptor has shown to be useful in terms of:

1. It uses the Curvelet transform to characterize brain regions and the Generalized Gaussian Distribution to reduce dimensionality.

2. It quantifies local-regional changes in brain regions by using a *2D multislice image*, aiming to capture local-regional edges and other singularities along brain curves in the Curvelet space and hence it sparsely describes atypical brain folding.

3. It is evaluated in heterogeneous sets of data which proves generalization.

In addition, at analyzing a 3D region by placing together each of the 3D slices in a plane, regional geometric 3D dependencies are characterized and quantified. Most of these

changes are usually masked in pathology conditions by conventional 3D measures like the volume or the equivalent curvature. This approach instead captures such relationships and express them in terms of local-regional geometric features which in addition are multiscale by nature. The rest of the discussion is organized in two parts: the relation between the identified relevant regions and the ASD, and a comparison between the obtained results and state-of-the-art strategies (including deep learning approaches).

The proposed Curvelet approach identified a set of relevant regions, most of them widely reported in the literature as relevant in ASD. Some studies have suggested Broca's and Wernicke's areas are commonly affected in ASD individuals, i.e., brain regions involved in producing and understanding language[44,45]. Parcelled regions within the Broca's area are revealed by the proposed descriptor, they are the parahippocampal gyrus, the inferior frontal gyrus, the fusiform cortex and the superior temporal gyrus, while those ones contained in the Wernicke's area are also identified with the Curvelet descriptor, they are the inferior frontal gyrus, the supramarginal gyrus and the angular gyrus. In addition, the proposed approach also distinguished the juxtapositional lobule cortex region, a part of the supplementary motor area, which has been reported to correlate with ASD[46].

Table 3 compares the results obtained using the proposed Curvelet approach against state-of-the-art methods (studies using ABIDE I). In this table, each row shows results for a particular method as follows: the first part (columns 2-4) presents information about the dataset and the last part (column 5) shows the computed AUC score per method. The proposed approach demonstrates to be competitive with state-of-the-art methods, yet this comparison is not completely fair since the validation sample is in general different. In consequence, for comparison purposes, most approaches took different cases, i.e., some of them built *homogeneous* samples (containing cases from a single center, a reduced number of centers or using the same scanner) or *non-homogeneous* samples (when the capturing conditions or centers are otherwise), being the latter our case.

Regarding homogeneous datasets, Retico *et al.*[14] collected a number of cases with their own scanner and characterized ASD using surface-based features, achieving AUC scores of 0.74 (male) and 0.68 (female), not shown in Table 3 since ABIDE is not used. Wang *et al.*[17] built a dataset by selecting subjects from a single center of ABIDE I (the NYU Langone Medical Center) and used a canonical correlation analysis over gray and white matter, obtaining

the best reported result, an AUC of 0.80 ± 0.02. Sato et al.[15] collected samples captured with the same scanner technology (Siemens 3T TimTrio). In this study, voxel-based morphometry methods were used for characterization and two classification tests were performed: using the whole brain and per region. The first test provided sensitivity of 0.58 and specificity of 0.72, while the second one reported sensitivity of 0.81 and specificity of 0.81 (using a set of regions reported to be part of the Social Network), not shown in Table 3 since ABIDE is not used. The task performed by these investigations is certainly much less difficult than ours since they decreased some variability sources yet the herein obtained classification performance is competitive with respect to the strategies aforementioned. Moreover, an additional test was performed using the proposed multiscale descriptor and a small set of data from ABIDE II (24 cases from a single center, the Kennedy Krieger Institute - KKI, 12 ASD patients and 12 control subjects) to carry out the binary classification under a 3-fold cross validation scheme, obtaining a maximum AUC of 0.88. This expected result was reached under similar experimentation conditions to whom have reported similar figures and, although under such restricted setup classification results do improve, such model may be hardly generalizable.

In terms of non-homogeneous datasets, Katuwal et al.[13] assessed a morphometry-based method by using an heterogeneous dataset, exhibiting low performance, an AUC of 0.60. Katuwal et al.[47] proposed a method that correlates morphometry features and patient data (e.g. age and verbal intelligence quotient), obtaining an AUC of 0.68. Interestingly, these works provide evidence about the influence of using heterogeneous dataset (high data variability). The proposed strategy can be included within this category since it was assessed using heterogeneous children samples from ABIDE, providing AUC scores of 0.75 and 0.77 for ABIDE I and II respectively, and 0.69 when training with ABIDE II and testing with ABIDE I. Following the same approach of using non-homogeneous data, a final test was performed by combining ABIDE I and ABIDE II samples into a single one and carrying out a 10-fold cross validation, obtaining an AUC of 0.75 and a set of relevant regions (most of them exactly the same described in Experiments 1 and 2). These results demonstrated the proposed approach is competitive w.r.t. baseline methods when using non-homogeneous datasets.

This last part of the discussion is devoted to the use of deep learning strategies, regardless of whether it is evaluated with homogeneous or non-homogeneous data. Note the following studies use other information sources and the T1-MRI. Parisot et al.[48] used a

Last edited $Date$: October 30, 2019

Graph Convolutional Network framework to detect anomalies associated to ASD by combining MRI and phenotypic data, reporting an AUC of 0.75. Akhavan et al.[49] trained a deep belief network with structural and functional MRI data of 185 individuals (between 5 to 10 years) from ABIDE, obtaining an accuracy of 0.65 (not shown in Table 3 since AUC score is not reported). Li et al.[50] used a deep transfer learning neural network with functional MRI data from 4 centers of ABIDE, obtaining a maximum AUC of 0.74. These studies basically demonstrated data availability (e.g. functional MRI, phenotypic data) plays a crucial role for ASD characterization since rather than a disease, this set of symptoms and signs is considered a disorder with a huge variability. The present analysis is nevertheless focused only in structural images, while most studies have mainly used brain representations from selected regions of interest (e.g. brain parcellations defined by anatomical atlases built by experts) to characterize the disease. Some deep learning approaches have aimed to find out anatomical landmarks to reduce the variability introduced by such particular brain parcellations[51,52]. Yet this might help to improve the automatic classification, its utility might be limited since these landmarks could hardly correlate with a functional meaning that helps out clinicians to improve their disease understanding and therefore patient management.

V.   Conclusions

This paper introduced a multiscale descriptor that uses a 2D representation and the Curvelet transform to characterize brain regions and identify those ones with differences between groups which ended up in the present investigation by being widely reported in the literature as characteristic of ASD, a side effect that may facilitate any ASD quantification. This work demonstrated the presented multiscale descriptor highlights different features and patterns when comparing with classic measures, probably local-global edges and discontinuities of spatial curves within the region. In addition, it also demonstrated to be competitive with respect to state-of-the-art strategies, including those based on the deep learning, evaluated with heterogeneous databases containing magnetic resonance images with differences in the number of slices per volume, in the inter-slice distance, in the image resolution and in the scanner protocol, i.e., robust to inter-center variability. Finally, the multiscale descriptor is simple in conceptual terms and shows a low computational cost when characterizing a MRI scan, approximately a quarter of a second. As a future work, a complete pipeline that

allows to perform a subject-wise classification is planned, as well as the inclusion of other sources of information to characterize ASD like neuropsychological tests, phenotypic data, and functional MRI examinations.

Acknowledgment

Conflict of interest disclosure

The authors have no conflicts to disclose.

References

[1]   M. M. T. Ismail, R. S. Keynton, M. M. M. O. Mostapha, A. H. ElTanboly, M. F. Casanova, G. L. Gimel'farb, and A. El-Baz, Studying Autism Spectrum Disorder with Structural and Diffusion Magnetic Resonance Imaging: A Survey, Frontiers in Human Neuroscience **10** (2016).

[2]   American Psychiatric Association et al., *Diagnostic and statistical manual of mental disorders (DSM-5)*, American Psychiatric Pub, 2013.

[3]   S. Ozonoff, A.-M. Iosif, F. Baguio, I. C. Cook, M. M. Hill, T. Hutman, S. J. Rogers, A. Rozga, S. Sangha, M. Sigman, M. B. Steinfeld, and G. S. Young, A Prospective Study of the Emergence of Early Behavioral Signs of Autism, Journal of the American Academy of Child & Adolescent Psychiatry **49**, 256–266.e2 (2010).

[4]   J. Baio et al., Prevalence of autism spectrum disorder among children aged 8

Last edited $Date$: October 30, 2019

years—autism and developmental disabilities monitoring network, 11 sites, United States, 2014, MMWR Surveillance Summaries **67**, 1 (2018).

[5] G. J. Blatt and S. H. Fatemi, Alterations in GABAergic Biomarkers in the Autism Brain: Research Findings and Clinical Implications, The Anatomical Record: Advances in Integrative Anatomy and Evolutionary Biology **294**, 1646–1652 (2011).

[6] Y. Lawrence, T. Kemper, M. Bauman, and G. Blatt, Parvalbumin-, calbindin-, and calretinin-immunoreactive hippocampal interneuron density in autism, Acta Neurologica Scandinavica **121**, 99–108 (2010).

[7] S. H. Fatemi, A. R. Halt, G. Realmuto, J. Earle, D. A. Kist, P. Thuras, and A. Merz, Purkinje cell size is reduced in cerebellum of patients with autism, Cellular and molecular neurobiology **22**, 171–175 (2002).

[8] M. L. Bauman and T. L. Kemper, Neuroanatomic observations of the brain in autism: a review and future directions, International Journal of Developmental Neuroscience **23**, 183–187 (2005).

[9] F. M. Vaccarino and K. M. Smith, Increased Brain Size in Autism—What It Will Take to Solve a Mystery, Biological Psychiatry **66**, 313–315 (2009).

[10] G. Auzias, M. Viellard, S. Takerkart, N. Villeneuve, F. Poinso, D. D. Fonséca, N. Girard, and C. Deruelle, Atypical sulcal anatomy in young children with autism spectrum disorder, NeuroImage: Clinical **4**, 593–603 (2014).

[11] M. F. Casanova, A. S. El-Baz, S. S. Kamat, B. A. Dombroski, F. Khalifa, A. Elnakib, A. Soliman, A. Allison-McNutt, and A. E. Switala, Focal cortical dysplasias in autism spectrum disorders, Acta Neuropathologica Communications **1**, 67 (2013).

[12] A. Giuliano, I. Gori, F. Muratori, I. Saviozzi, P. Oliva, R. Tancredi, A. Cosenza, M. Tosetti, S. Calderoni, and A. Retico, Machine learning techniques implemented ON structural MRI features at different spatial scales for preschoolers with autism spectrum disorders, Physica Medica **32**, 128 (2016).

[13] G. J. Katuwal, N. D. Cahill, S. A. Baum, and A. M. Michael, The predictive power of structural MRI in Autism diagnosis, in *2015 37th Annual International Conference of the IEEE Engineering in Medicine and Biology Society (EMBC)*, IEEE, 2015.

Last edited $Date$: October 30, 2019

[14] A. Retico, I. Gori, A. Giuliano, F. Muratori, and S. Calderoni, One-Class Support Vector Machines Identify the Language and Default Mode Regions As Common Patterns of Structural Alterations in Young Children with Autism Spectrum Disorders, Frontiers in Neuroscience **10** (2016).

[15] W. Sato, T. Kochiyama, S. Uono, S. Yoshimura, Y. Kubota, R. Sawada, M. Sakihama, and M. Toichi, Reduced Gray Matter Volume in the Social Brain Network in Adults with Autism Spectrum Disorder, Frontiers in Human Neuroscience **11** (2017).

[16] A. Chaddad, C. Desrosiers, and M. Toews, Multi-scale radiomic analysis of sub-cortical regions in MRI related to autism, gender and age, Scientific Reports **7** (2017).

[17] L. Wang, C. Y. Wee, X. Tang, P. T. Yap, and D. Shen, Multi-task feature selection via supervised canonical graph matching for diagnosis of autism spectrum disorder, Brain Imaging and Behavior **10**, 33–40 (2015).

[18] A. Di Martino et al., The autism brain imaging data exchange: towards a large-scale evaluation of the intrinsic brain architecture in autism, Molecular psychiatry **19**, 659 (2014).

[19] A. Di Martino et al., Enhancing studies of the connectome in autism using the autism brain imaging data exchange II, Scientific data **4**, 170010 (2017).

[20] E. R. Whitney, T. L. Kemper, D. L. Rosene, M. L. Bauman, and G. J. Blatt, Density of cerebellar basket and stellate cells in autism: Evidence for a late developmental loss of Purkinje cells, Journal of Neuroscience Research **87**, 2245–2254 (2009).

[21] E. R. Whitney, T. L. Kemper, M. L. Bauman, D. L. Rosene, and G. J. Blatt, Cerebellar Purkinje Cells are Reduced in a Subpopulation of Autistic Brains: A Stereological Experiment Using Calbindin-D28k, The Cerebellum **7**, 406–416 (2008).

[22] M. Jenkinson, C. F. Beckmann, T. E. Behrens, M. W. Woolrich, and S. M. Smith, Fsl, Neuroimage **62**, 782–790 (2012).

[23] S. M. Smith, Fast robust automated brain extraction, Human Brain Mapping **17**, 143–155 (2002).

Last edited $Date$: October 30, 2019

24 M. Jenkinson, P. Bannister, M. Brady, and S. Smith, Improved Optimization for the Robust and Accurate Linear Registration and Motion Correction of Brain Images, NeuroImage **17**, 825–841 (2002).

25 J. L. Andersson et al., Non-linear registration, aka Spatial Normalisation FMRIB technical report TR07JA2, FMRIB Analysis Group of the University of Oxford **2**, 1–21 (2007).

26 N. Makris, J. M. Goldstein, D. Kennedy, S. M. Hodge, V. S. Caviness, S. V. Faraone, M. T. Tsuang, and L. J. Seidman, Decreased volume of left and total anterior insular lobule in schizophrenia, Schizophrenia Research **83**, 155–171 (2006).

27 Y. Jiao, R. Chen, X. Ke, K. Chu, Z. Lu, and E. H. Herskovits, Predictive models of autism spectrum disorder based on brain regional cortical thickness, NeuroImage **50**, 589–599 (2010).

28 B. F. Sparks, S. D. Friedman, D. W. Shaw, E. H. Aylward, D. Echelard, A. A. Artru, K. R. Maravilla, J. N. Giedd, J. Munson, G. Dawson, and S. R. Dager, Brain structural abnormalities in young children with autism spectrum disorder, Neurology **59**, 184–192 (2002).

29 E. J. Candes and D. L. Donoho, Curvelets: A surprisingly effective nonadaptive representation for objects with edges, Technical report, Stanford Univ Ca Dept of Statistics, 2000.

30 M. Do and M. Vetterli, Wavelet-based texture retrieval using generalized Gaussian density and Kullback-Leibler distance, IEEE Transactions on Image Processing **11**, 146–158 (2002).

31 E. Candes, L. Demanet, D. Donoho, and L. Ying, Fast Discrete Curvelet Transforms, Multiscale Modeling & Simulation **5**, 861–899 (2006).

32 D. R. Larson, P. Massopust, Z. Nashed, M. C. Nguyen, M. Papadakis, and A. Zayed, editors, *Frames and Operator Theory in Analysis and Signal Processing*, American Mathematical Society, 2008.

[33] F. Gómez and E. Romero, Rotation invariant texture characterization using a curvelet based descriptor, Pattern Recognition Letters **32**, 2178–2186 (2011).

[34] P. J. Davis, Leonhard Euler's integral: A historical profile of the Gamma function: In memoriam: Milton Abramowitz, The American Mathematical Monthly **66**, 849–869 (1959).

[35] C. Cortes and V. Vapnik, Support-vector networks, Machine learning **20**, 273–297 (1995).

[36] J. Snoek, H. Larochelle, and R. P. Adams, Practical bayesian optimization of machine learning algorithms, in *Advances in neural information processing systems*, pages 2951–2959, 2012.

[37] L. L. Sears, C. Vest, S. Mohamed, J. Bailey, B. J. Ranson, and J. Piven, An MRI study of the basal ganglia in autism, Progress in Neuro-Psychopharmacology and Biological Psychiatry **23**, 613–624 (1999).

[38] J. A. Bastiaansen, M. Thioux, L. Nanetti, C. van der Gaag, C. Ketelaars, R. Minderaa, and C. Keysers, Age-Related Increase in Inferior Frontal Gyrus Activity and Social Functioning in Autism Spectrum Disorder, Biological Psychiatry **69**, 832–838 (2011).

[39] J. Liu et al., Gray matter abnormalities in pediatric autism spectrum disorder: a meta-analysis with signed differential mapping, European child & adolescent psychiatry **26**, 933–945 (2017).

[40] E. D. Bigler, S. Mortensen, E. S. Neeley, S. Ozonoff, L. Krasny, M. Johnson, J. Lu, S. L. Provencal, W. McMahon, and J. E. Lainhart, Superior Temporal Gyrus, Language Function, and Autism, Developmental Neuropsychology **31**, 217–238 (2007).

[41] A. D. Martino, C. Kelly, R. Grzadzinski, X.-N. Zuo, M. Mennes, M. A. Mairena, C. Lord, F. X. Castellanos, and M. P. Milham, Aberrant Striatal Functional Connectivity in Children with Autism, Biological Psychiatry **69**, 847–856 (2011).

[42] B. Fischl, Automatically Parcellating the Human Cerebral Cortex, Cerebral Cortex **14**, 11–22 (2004).

Last edited $Date$: October 30, 2019

43 B. Fischl and A. M. Dale, Measuring the thickness of the human cerebral cortex from magnetic resonance images, Proceedings of the National Academy of Sciences **97**, 11050–11055 (2000).

44 T. A. KNAUS, A. M. SILVER, K. A. LINDGREN, N. HADJIKHANI, and H. TAGER-FLUSBERG, fMRI activation during a language task in adolescents with ASD, Journal of the International Neuropsychological Society **14**, 967–979 (2008).

45 A. Yasuhara, Correlation between EEG abnormalities and symptoms of autism spectrum disorder (ASD), Brain and Development **32**, 791–798 (2010).

46 I. Puzzo, N. R. Cooper, P. Vetter, and R. Russo, EEG activation differences in the pre-motor cortex and supplementary motor area between normal individuals with high and low traits of autism, Brain Research **1342**, 104–110 (2010).

47 G. J. Katuwal, S. A. Baum, N. D. Cahill, and A. M. Michael, Divide and Conquer: Sub-Grouping of ASD Improves ASD Detection Based on Brain Morphometry, PLOS ONE **11**, e0153331 (2016).

48 S. Parisot, S. I. Ktena, E. Ferrante, M. Lee, R. Guerrero, B. Glocker, and D. Rueckert, Disease prediction using graph convolutional networks: Application to Autism Spectrum Disorder and Alzheimer's disease, Medical Image Analysis **48**, 117–130 (2018).

49 M. A. Aghdam, A. Sharifi, and M. M. Pedram, Combination of rs-fMRI and sMRI Data to Discriminate Autism Spectrum Disorders in Young Children Using Deep Belief Network, Journal of Digital Imaging **31**, 895–903 (2018).

50 H. Li, N. A. Parikh, and L. He, A Novel Transfer Learning Approach to Enhance Deep Neural Network Classification of Brain Functional Connectomes, Frontiers in Neuroscience **12** (2018).

51 M. Liu, J. Zhang, D. Nie, P.-T. Yap, and D. Shen, Anatomical Landmark Based Deep Feature Representation for MR Images in Brain Disease Diagnosis, IEEE Journal of Biomedical and Health Informatics **22**, 1476–1485 (2018).

52 M. Liu, J. Zhang, E. Adeli, and D. Shen, Landmark-based deep multi-instance learning for brain disease diagnosis, Medical Image Analysis **43**, 157–168 (2018).

Last edited $Date$: October 30, 2019

List of Figure legends:

- **Figure 1.** The proposed strategy consists in three phases. In (A) each case is pre-processed to normalize image intensities, remove the skull and segment the brain into a set of anatomical regions. In (B) the multiscale descriptor is computed by transforming each segmented region into a 2D multislice image, applying a multiscale analysis with the Curvelet transform and approximating each Curvelet sub-band coefficient distribution by a Generalized Gaussian Distribution to reduce dimensionality. Finally in (C) a conventional classification is performed per region to assess the robustness of the feature descriptor in differentiating ASD patients from control subjects.

- **Figure 2.** Description of a brain region given the 2D multislice image representation. From top to bottom, the mosaic (2D multiscale image) is taken as an input for computing the Curvelet transform, whose coefficients are displayed at the center panel, and at the bottom, histograms of three sub-bands are shown as well as their distribution estimations.

- **Figure 3.** Classification results when the model is trained using the ABIDE II sample and tested using the ABIDE I. At the top, each brain illustrates regions with the highest AUC scores obtained with an RBF and a linear kernel, respectively. At the bottom, the corresponding AUC scores are presented with the color code associated to each brain region. Abbreviations: right (R), left (L), cortex (C), anterior division (AD), posterior division (PD), pars triangularis (PT).

- **Figure 4.** Discriminant regions when evaluating the proposed multiscale descriptor with the ABIDE I sample: the upper two brains stand for an RBF kernel while the bottom ones represent a linear kernel. The corresponding AUC scores and the associated standard deviations are displayed in the legend. The color code associated to the set of relevant regions is also displayed. Abbreviations: right (R), left (L), cortex (C), temporal (T), anterior division (AD), pars triangularis (PT).

- **Figure 5.** Discriminant regions when evaluating the proposed approach with the ABIDE II sample: the same set of brain region was obtained using an RBF or a linear kernel. Color code is in this case different since the identified regions are not exactly the same as the ones resulting when evaluating with the ABIDE I sample. Notice just

Last edited $Date$: October 30, 2019

one discriminant sub-cortical region was obtained. Abbreviations: right (R), left (L), cortex (C), anterior division (AD), posterior division (PD).

- **Figure 6.** A: the right supramarginal gyrus (anterior division) while B: the left superior temporal gyrus (anterior division). For each block, first two columns illustrate the original volume of the selected region and the third column shows the reconstructed region volume after using a particular sub-band. Each volume represents a subject of a particular class, i.e., ASD patients (orange) or control subjects (blue).

- **Figure 7.** Curvelet-based feature analysis. Each column represents a Curvelet sub-band, while the rows stand for: control and autism groups (first), the control and autism groups distributed by age ranges (second), and the control and autism groups distributed by scanner/center (third). Green color corresponds to autism spectrum disorder patients (ASD) while orange corresponds to controls subjects (CNT).

- **Figure 8.** Relationship between three Curvelet sub-bands (each column) and classical measures like normalized volume (first row), thickness (second row) and curvature (third row).

- **Table 1.** Data description: ABIDE I and II samples.

- **Table 2.** From left to right, relevant regions with the HO atlas obtained with Curvelet approach (first), AUC scores when using the Curvelet approach (second) and the normalized volume (third), approximated regions from the DKT atlas that correlate with the HO atlas (forth), AUC scores when using the thickness (fifth) and the curvature (sixth). Abbreviations: left (L), right (R), gyrus (G), cortex (C).

- **Table 3.** Comparison between results obtained with the proposed approach and state of the art methods assessed with ABIDE dataset. Abbreviations: control (CRT), autism spectrum disorders (ASD), area under the receiver operator curve (AUC).

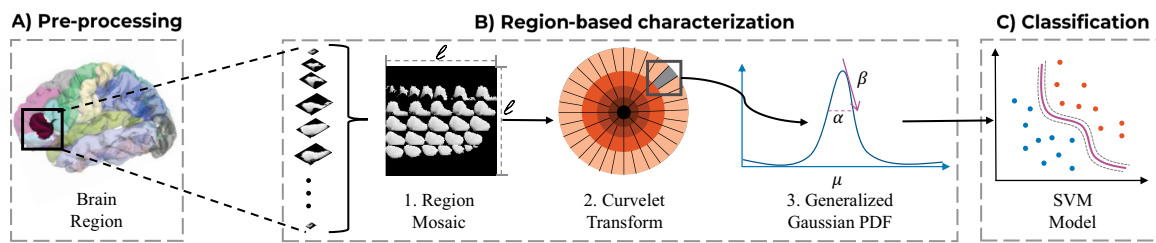Last edited $Date$: October 30, 2019

Figure 1: The proposed strategy consists in three phases. In (A) each case is pre-processed to normalize image intensities, remove the skull and segment the brain into a set of anatomical regions. In (B) the multiscale descriptor is computed by transforming each segmented region into a 2D multislice image, applying a multiscale analysis with the Curvelet transform and approximating each Curvelet sub-band coefficient distribution by a Generalized Gaussian Distribution to reduce dimensionality. Finally in (C) a conventional classification is performed per region to assess the robustness of the feature descriptor in differentiating ASD patients from control subjects.

Table 1: Data description: ABIDE I and II samples

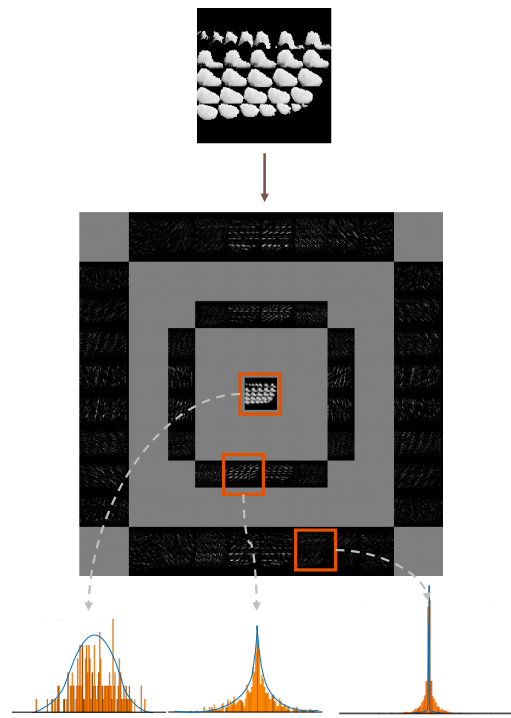| Site	ABIDE I			ABIDE II			Scanner Tech.
	ASD	CNT	Tot.	ASD	CNT	Tot.	
Max Mun	8	5	13				Siemens Magnetom Verio
Olin	2	2	4				Siemens Magnetom Allegra
SDSU	5	6	11	10	1	11	GE 3T MR750
Trinity	6	6	12				Philips 3T Achieva
Yale	13	14	27				Siemens Magnetom Trio
KKI	0	1	1	12	27	39	Philips 3T Achieva
GU				17	11	28	Siemens 3T Trio
UCD				3	2	5	Siemens 3T Trio
Total	**34**	**34**	**68**	**42**	**41**	**83**	

Last edited $Date$: October 30, 2019

Figure 2: Description of a brain region given the 2D multislice image representation. From top to bottom, the mosaic (2D multiscale image) is taken as an input for computing the Curvelet transform, whose coefficients are displayed at the center panel, and at the bottom, histograms of three sub-bands are shown as well as their distribution estimations.

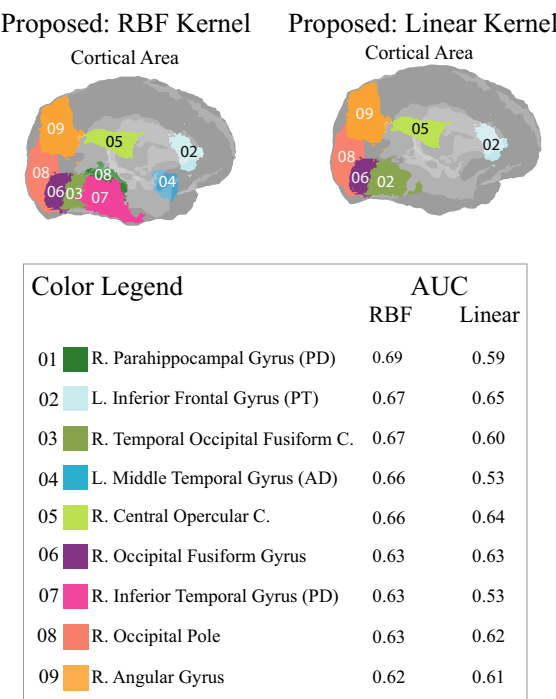| Color Legend		AUC	
		RBF	Linear
01 ▮ R. Parahippocampal Gyrus (PD)		0.69	0.59
02 ▮ L. Inferior Frontal Gyrus (PT)		0.67	0.65
03 ▮ R. Temporal Occipital Fusiform C.		0.67	0.60
04 ▮ L. Middle Temporal Gyrus (AD)		0.66	0.53
05 ▮ R. Central Opercular C.		0.66	0.64
06 ▮ R. Occipital Fusiform Gyrus		0.63	0.63
07 ▮ R. Inferior Temporal Gyrus (PD)		0.63	0.53
08 ▮ R. Occipital Pole		0.63	0.62
09 ▮ R. Angular Gyrus		0.62	0.61

Figure 3: Classification results when the model is trained using the ABIDE II sample and tested using the ABIDE I. At the top, each brain illustrates regions with the highest AUC scores obtained with an RBF and a linear kernel, respectively. At the bottom, the corresponding AUC scores are presented with the color code associated to each brain region. Abbreviations: right (R), left (L), cortex (C), anterior division (AD), posterior division (PD), pars triangularis (PT).

Proposed: RBF Kernel

Cortical Area · Sub-Cortical Area

Proposed: Linear Kernel

Cortical Area · Sub-Cortical Area

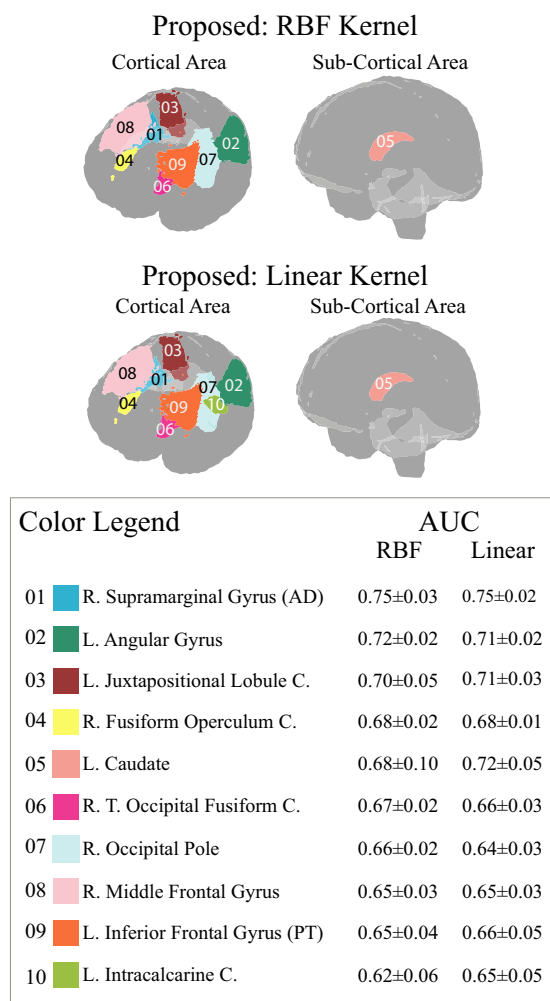| Color Legend	AUC	
	RBF	Linear
01 R. Supramarginal Gyrus (AD)	0.75±0.03	0.75±0.02
02 L. Angular Gyrus	0.72±0.02	0.71±0.02
03 L. Juxtapositional Lobule C.	0.70±0.05	0.71±0.03
04 R. Fusiform Operculum C.	0.68±0.02	0.68±0.01
05 L. Caudate	0.68±0.10	0.72±0.05
06 R. T. Occipital Fusiform C.	0.67±0.02	0.66±0.03
07 R. Occipital Pole	0.66±0.02	0.64±0.03
08 R. Middle Frontal Gyrus	0.65±0.03	0.65±0.03
09 L. Inferior Frontal Gyrus (PT)	0.65±0.04	0.66±0.05
10 L. Intracalcarine C.	0.62±0.06	0.65±0.05

Figure 4: Discriminant regions when evaluating the proposed multi-scale descriptor with the ABIDE I sample: the upper two brains stand for an RBF kernel while the bottom ones represent a linear kernel. The corresponding AUC scores and the associated standard deviations are displayed in the legend. The color code associated to the set of relevant regions is also displayed. Abbreviations: right (R), left (L), cortex (C), temporal (T), anterior division (AD), pars triangularis (PT).

Proposed: Both Kernels

Cortical Area   Sub-Cortical Area

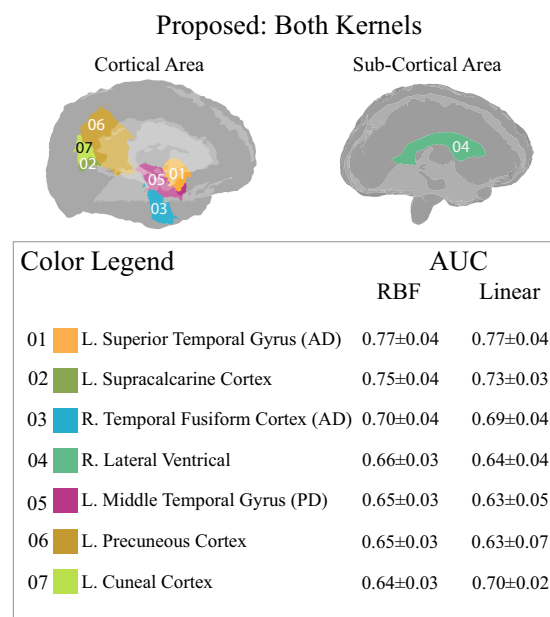| Color Legend			AUC	
			RBF	Linear
01		L. Superior Temporal Gyrus (AD)	0.77±0.04	0.77±0.04
02		L. Supracalcarine Cortex	0.75±0.04	0.73±0.03
03		R. Temporal Fusiform Cortex (AD)	0.70±0.04	0.69±0.04
04		R. Lateral Ventrical	0.66±0.03	0.64±0.04
05		L. Middle Temporal Gyrus (PD)	0.65±0.03	0.63±0.05
06		L. Precuneous Cortex	0.65±0.03	0.63±0.07
07		L. Cuneal Cortex	0.64±0.03	0.70±0.02

Figure 5: Discriminant regions when evaluating the proposed approach with the ABIDE II sample: the same set of brain region was obtained using an RBF or a linear kernel. Color code is in this case different since the identified regions are not exactly the same as the ones resulting when evaluating with the ABIDE I sample. Notice just one discriminant sub-cortical region was obtained. Abbreviations: right (R), left (L), cortex (C), anterior division (AD), posterior division (PD).
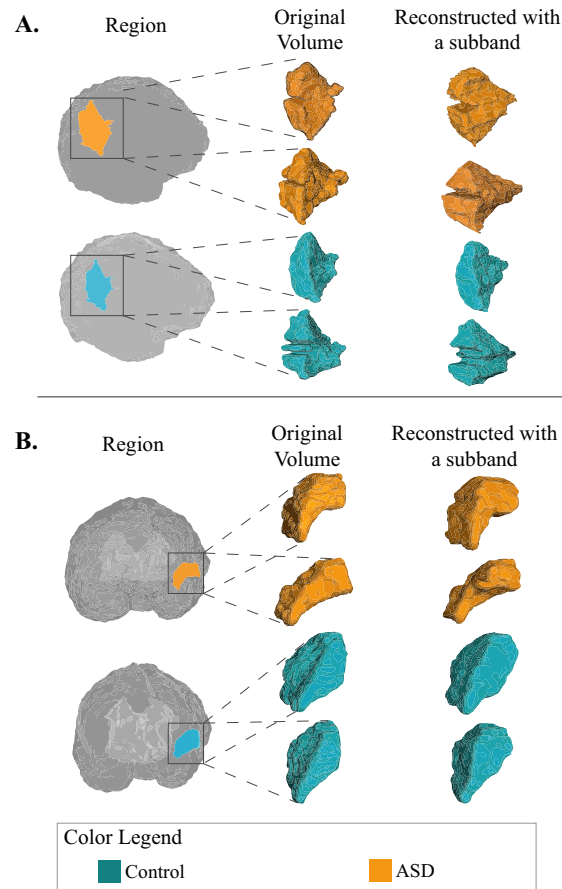
Figure 6: A: the right supramarginal gyrus (anterior division) while B: the left superior temporal gyrus (anterior division). For each block, first two columns illustrate the original volume of the selected region and the third column shows the reconstructed region volume after using a particular sub-band. Each volume represents a subject of a particular class, i.e., ASD patients (orange) or control subjects (blue).
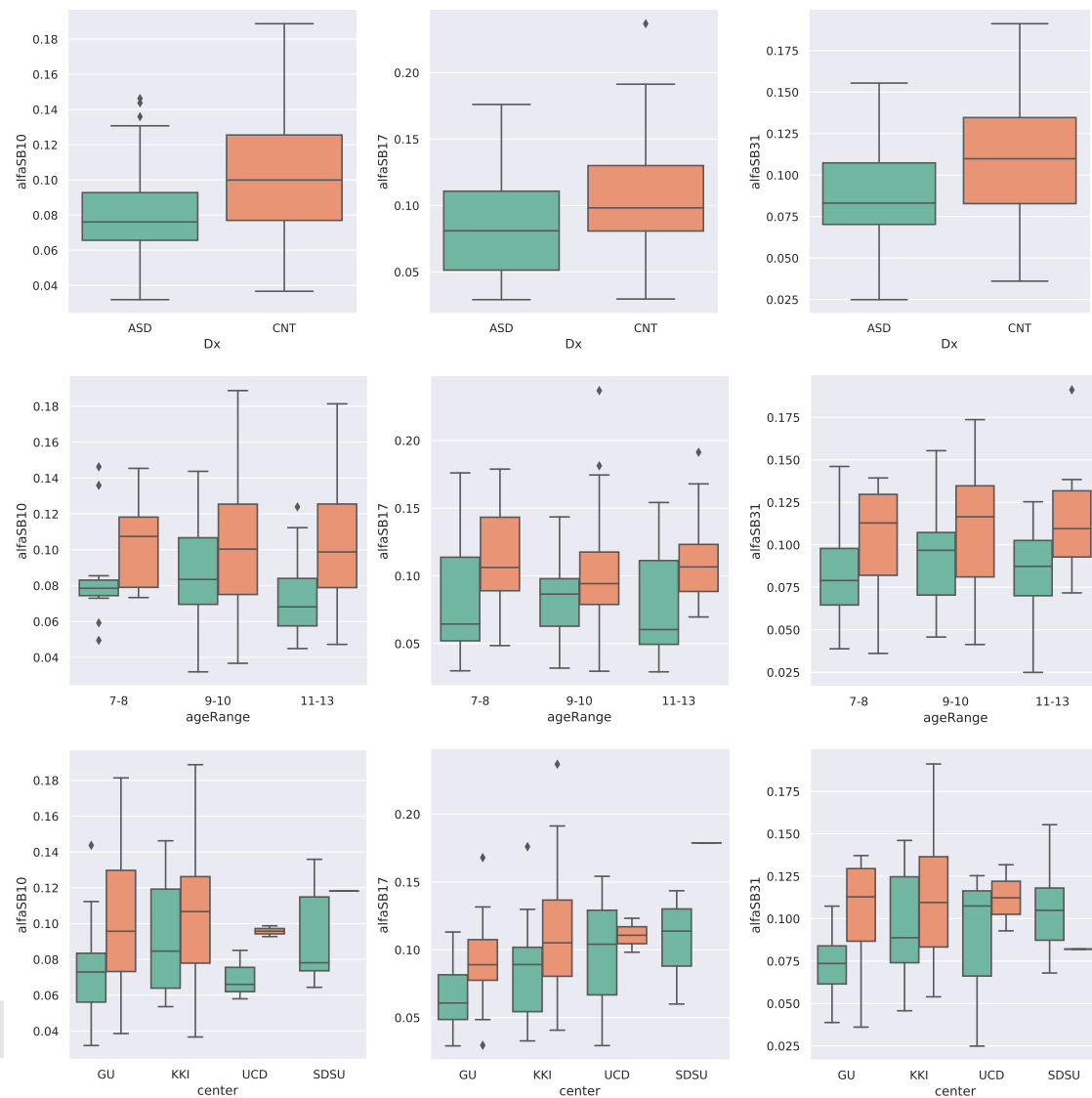
Figure 7: Curvelet-based feature analysis. Each column represents a Curvelet sub-band, while the rows stand for: control and autism groups (first), the control and autism groups distributed by age ranges (second), and the control and autism groups distributed by scanner/center (third). Green color corresponds to autism spectrum disorder patients (ASD) while orange corresponds to controls subjects (CNT).
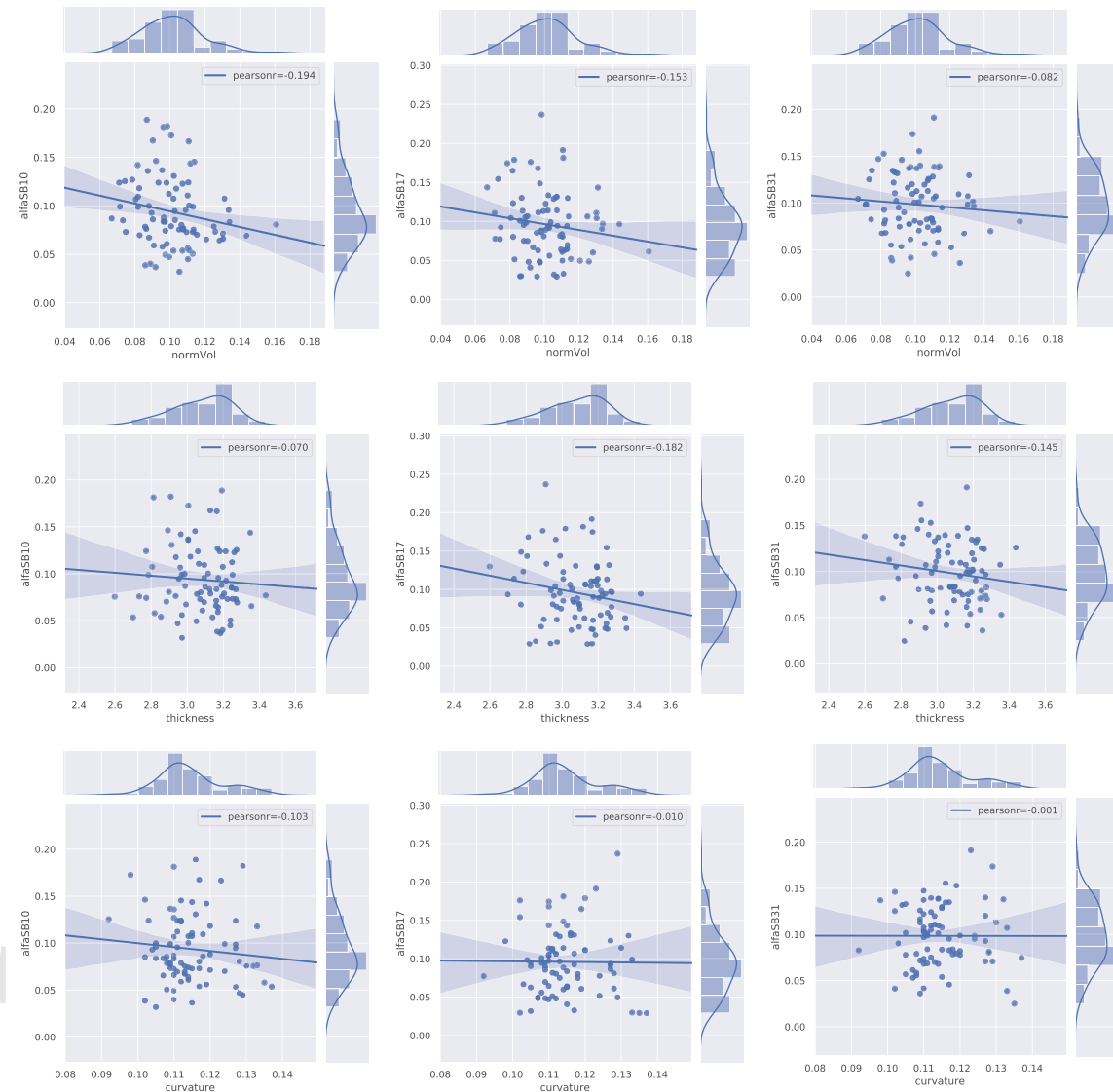
Figure 8: Relationship between three Curvelet sub-bands (each column) and classical measures like normalized volume (first row), thickness (second row) and curvature (third row).

Table 2: From left to right, relevant regions with the Harvard Oxford (HO) atlas obtained with Curvelet approach (first), AUC scores when using the Curvelet approach (second) and the normalized volume (third), approximated regions from the Desikan Killiany (DKT) atlas that correlate with the HO atlas (forth), AUC scores when using the thickness (fifth) and the curvature (sixth). Abbreviations: proposed strategy (Prop), normalize volume (Vol), thickness (Thick), curvature (Curv), left (L), right (R), gyrus (G), cortex (C).

Regions HO Atlas	AUC Prop	AUC Vol	Regions DKT Atlas	AUC Thick	AUC Curv
L. Superior Temporal G.	**0.77**	0.61	L. Superior Temporal	0.51	0.55
L. Supra calcarine C.	**0.75**	0.51	L. Peri calcarine	0.65	0.49
L. Middle Temporal G.	**0.71**	0.52	L. Middle Temporal	0.53	0.66
R. Temporal Fusiform C.	**0.71**	0.49	R. Fusiform	0.34	0.55
L. Inferior Temporal G.	**0.67**	0.56	L. Inferior Temporal	0.43	0.67
L. Precu- neous C.	**0.67**	0.56	L. Precuneus	0.56	0.59
R. Para hippo- campal G.	**0.67**	0.42	R. Para hippocampal	0.53	0.62
L. Cuneal C.	**0.66**	0.56	L. Cuneus	0.51	0.44
L. Temporal Fusiform C.	**0.65**	0.53	L. Fusiform	0.50	0.60

Table 3: Comparison between results obtained with the proposed approach and state of the art methods assessed with ABIDE dataset. Abbreviations: control (CRT), autism spectrum disorders (ASD), area under the receiver operator curve (AUC).

	CNT	ASD	Age	AUC
Wang[17]	54	57	<15	0.80 *
Katuwal[13]	373	371	NR	0.60
Katuwal[47]	361	373	7 - 64	0.68
Parisot[48]	468	403	6 to 64	0.75
Li[50]	149	161	10 to 34	0.74
Proposed	151	151	6 - 13	0.75 0.77 **

* This result was obtained with cases from a single center: the NYU Langone Medical Center.
** This result corresponds to Tests 2.a and 2.b.